

Utilizing Toray Paper as a Metal-Free, High Surface Area Electrode for Photosystem I–Driven Mediated Electron Transfer

Christopher D. Stachurski, John M. Williams, Pamela M. Tabaquin, Elisabeth D. Wood, Nsoki Phambu, G. Kane Jennings, and David E. Cliffl*^{*}

One challenge in capitalizing on the affordability, sustainability, and accessibility of biohybrid solar energy conversion, including devices based on Photosystem I (PSI), is the identification of metal-free electrode materials to replace the inorganic substrates commonly found in solar cell development. Herein, commercially available Toray carbon paper (CP) is investigated as a high surface area, carbon electrode for the development of photoactive bioelectrodes consisting of PSI and poly(3,4-ethylenedioxythiophene) polystyrene sulfonate (PEDOT:PSS). Mediated anodic photocurrent is achieved at both PSI multilayer and PSI–polymer composite films on CP electrodes subjected to flame pre-treatment. Film preparation is optimized by utilizing potential sweep voltammetry in place of potentiostatic conditions for polymerization. The optimized PSI–PEDOT:PSS films achieve a threefold increase in polymer growth under potential sweep conditions, quantified through net charge consumed during electropolymerization, resulting in a fourfold increase in photocurrent density (-53 vs -196 nA cm⁻²). The ability to prepare photoactive PSI-polymer films on metal-free CP electrodes opens the door to a rapidly scalable system for biohybrid energy production ultimately leading to more affordable, sustainable, and accessible energy.

protein complex Photosystem I (PSI), has been of particular interest due to its high efficiency and natural role as a photodiode. These properties have made PSI a promising candidate for use in conventional energy-harvesting systems and continue to inspire biohybrid research to this day.^[4–6]

This roughly 500 kDa protein is primarily composed of a large array of chlorophyll surrounding an electron-transport chain that begins at a chlorophyll dimer at the center of the protein (P₇₀₀) and travels through a series of phyloquinone mediators before arriving at a terminal iron–sulfur complex (F_B) where it is then accessible for transfer to external charge carriers.^[7,8] The protein absorbs a wide range of solar energy due to the chlorophyll array and is capable of exciton generation of nearly -1.2 eV with low-energy (>600 nm) light. At F_B, electrons are transferred with energy of -3.9 eV compared to vacuum, making excitons energetically compatible with numerous materials, ranging from metals to semimetals to semiconductors.^[9,10] Despite the efficiency of

inorganic electrode materials, an overreliance on precious metal-based substrates ultimately limits the sustainability and affordability of PSI-based devices.

Recent studies have investigated carbon materials as alternatives to inorganic electrodes in PSI biohybrid solar cells.^[11–14] Carbon materials exhibit high conductivities, diverse morphologies, and increased affordability over metal-based substrates promoting their rapid incorporation into biohybrid energy applications. Many

1. Introduction

Rising environmental concerns have sparked interest in diversifying sources of renewable green energy over the past few decades. Biohybrid sources of energy, or those motivated by materials and processes found in nature, have pushed the idea of “green energy” even further by relying on components with low environmental and economic costs.^[1–3] One such material, the photosynthetic

C. D. Stachurski, E. D. Wood, D. E. Cliffl
Department of Chemistry
Vanderbilt University
7300 Stevenson Center Lane, Nashville, TN 37235-1822, USA
E-mail: d.cliffl@vanderbilt.edu

J. M. Williams
Interdisciplinary Materials Science & Engineering
Vanderbilt University
7300 Stevenson Center Lane, Nashville, TN 37235-1822, USA

 The ORCID identification number(s) for the author(s) of this article can be found under <https://doi.org/10.1002/ente.202201077>.

DOI: 10.1002/ente.202201077

P. M. Tabaquin
Department of Chemistry
Queensborough Community College
222-05 56th Avenue, Bayside, NY 11364-1432, USA

N. Phambu
Department of Chemistry
Tennessee State University
3500 John A. Merritt Boulevard, Nashville, TN 37209-1500, United States

G. K. Jennings
Department of Chemical and Biomolecular Engineering
Vanderbilt University
2301 Vanderbilt Place, Nashville, TN 37235-1604, USA

carbon allotropes are also amenable to upscaling alongside PSI as a means of device enhancement. Gunther et al. demonstrated how graphene could interface with monolayers of PSI for sustained anodic photocurrent production in the presence of diffusible chemical mediators.^[15] Darby et al. expanded upon this work by substituting in reduced graphene oxide to facilitate higher amounts of PSI loading and lead to upward of $5 \mu\text{A cm}^{-2}$ of observed photocurrent.^[16] Beyond planar allotropes of carbon, Ciornii et al. utilized multiwalled carbon nanotubes as a scaffold for PSI immobilization through the use of the redox protein cytochrome C (cyt C) to produce up to $18 \mu\text{A cm}^{-2}$ at biased electrodes.^[17] More recently, Morlock et al. created 3D structures of reduced graphene oxide capable of similar cyt C-assisted immobilization of PSI, leading to high photocurrents ($14 \mu\text{A cm}^{-2}$) and high rates of protein turnover ($30 \text{ e}^- \text{ PSI}^{-1} \text{ s}^{-1}$).^[18] Despite these successes, past uses of carbon allotropes in PSI biohybrid devices are often layered on conventional electrodes, such as gold, silicon, or glassy carbon, restricting the benefits of affordable, sustainable, and scalable carbon materials. Some devices replace electrode materials with insulating supports; however, additional processing steps serve as barriers to upscaling and affordable device architectures requiring further optimization before truly green energy is achieved.

Carbon paper (CP) is a promising electrode candidate for biohybrid photoelectrochemical cells due to inherently high surface area and conductivity.^[11,13] Past work by Rasmussen et al. demonstrated how CP has been employed as an electrode in whole thylakoid devices capable of highly sensitive herbicide detection using spinach-extracted thylakoids.^[19,20] The high surface area of CP substrates makes them promising candidates for PSI-polymer composites prepared using electropolymerization.^[21–25] Protein-polymer composites have demonstrated improved structural and photoelectrochemical performance despite lower-than-average quantities of protein due to favorable interactions between the conducting polymer and terminal reaction centers of PSI. Robinson et al. successfully encapsulated PSI multilayers within a vapor-phase-polymerized poly(3,4-ethylenedioxythiophene) (PEDOT) scaffold which produced high-activity composite films resistant to delamination. Gizzie et al. employed a solution of PSI and aniline monomer to rapidly grow photoactive films on planar gold electrodes, showing that the entrapped PSI outperformed more dense multilayers prepared in the absence of polyaniline (PANi).^[21] Yet planar electrodes have shown limitations in electropolymerization processes as diminishing returns are observed beyond critical film thicknesses.^[21] These limiting factors can be overcome by using 3D electrodes that offer significantly higher electrode surface areas per geometric area, which enables significantly more electropolymerization before desorption limits any additional growth.^[26,27]

In this work, PSI is interfaced with CP electrodes either through physical adsorption or entrapment in conducting polymers formed in situ. Following preconditioning, the treated CP electrodes exhibit much improved hydrophilicity, which in turn increases the electrode surface areas and leads to the formation of dense electro-active layers. The prepared PSI or PSI-polymer films are assembled by using different procedures and tested in the presence of multiple chemical mediators to identify the optimal conditions for devices of this nature. Optimal devices generated up to 220 nA cm^{-2} of anodic governed by diffusion-limited pathways rather than kinetic limitations at the electrode. The composition and preparation of

CP-based bioelectrodes prepared in this study opens the door to rapidly scalable device assembly unhindered by the limitations tied to systems based on inorganic materials and can lead to truly sustainable sources of renewable energy.

2. Results and Discussion

2.1. Toray Paper Electrode Preparation

Many CP substrates are prepared for applications as gas permeation membranes and, as such, often come pretreated with a hydrophobic polytetrafluoroethylene (PTFE) coating making them inherently incompatible with aqueous electrochemical systems. To prepare the electrodes for use in PSI biohybrid devices, CP substrates were pretreated by either chemical oxidation using sulfuric acid or flame treated using a Bunsen burner prior to use in electrochemical applications. By first wetting the substrate with ethanol followed by a brief (5 min) exposure to sulfuric acid, the wettability of the CP substrate (AT-CP) was significantly enhanced as shown by the change in contact angle from $122 \pm 4^\circ$ to $24 \pm 2^\circ$ (Figure 1A). More extreme surface modification was achieved through flame treatment and the resulting substrate (flame-treated carbon paper [FT-CP]) was fully wettable ($\Theta < 5^\circ$) posing no barrier to interaction with PSI-containing solutions.

This improved hydrophilicity is attributed to simultaneously increasing the physical roughness of CP fibers, as evident in SEM images pre- and posttreatment (Figure S1, Supporting Information), removing the PTFE coating, and increasing functionalized sp^3 carbon as evidenced in the resulting Raman spectra (Figure 1B). Over the two treatment methods applied to CP substrates, the ratio of the D-band ($\approx 1356 \text{ cm}^{-1}$) to the G-band ($\approx 1585 \text{ cm}^{-1}$), comprising signal from sp^3 and sp^2 carbon, respectively, increased from 0.13 (CP) to 0.26 (AT-CP) to 0.60 (FT-CP). Increased sp^3 hybridized carbon at the electrode improves surface polarity, and in turn, leads to an increasingly hydrophilic substrate. This finding is consistent with the results Choi et al., who sonicated commercial CP in a mixture of concentrated sulfuric and nitric acid to improve the adhesion of PANi grown in situ.^[28]

Electrochemical characterization was used to measure changes in the electroactive surface area, likely a result of improved CP hydrophilicity following surface pretreatment. Cyclic voltammograms (CVs) of CP substrates treated using different methods show increased faradaic and non-faradaic current responses over those without any form of modification. Increased faradaic responses, demonstrated with the dissolved mediator hexaammineruthenium (III) chloride (RuHex) at CP electrodes that underwent more intense pretreatment, demonstrate superior electroactive surface areas when compared to untreated CP or planar glassy carbon (Figure 1C).

Peak currents (I_p) for the FT-CP increased by factors of 6 and 9 for the observed oxidation and 3 and 11 for the observed reduction reaction, with respect to untreated CP and glassy carbon controls. These results, in conjunction with the observed increase in hydrophilicity, suggest that the applied treatment methods allow more of the available surface area of the CP substrates to be

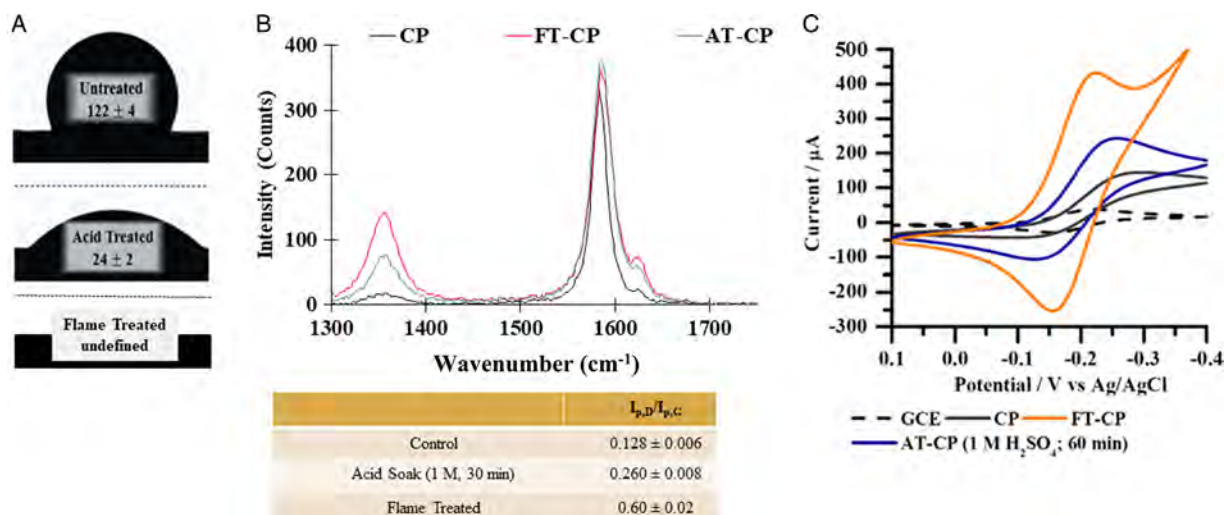


Figure 1. A) Contact-angle measurement showing decreased hydrophobicity of flame-treated and acid-treated carbon paper (CP) electrodes compared to untreated controls. B) Raman spectra of untreated, acid-treated, and flame-treated CP electrodes with the calculated ratios of the peak intensity of the D and G bands. Following flame treatment, the I_D/I_G increases from 0.13 to 0.60 representing an increase in sp^3 -functionalized carbon at the substrate surface. C) Cyclic voltammograms at 100 mV s^{-1} of untreated CP, CP treated with $1 \text{ M H}_2\text{SO}_4$ for 60 min (AT-CP), flame-treated CP (FT-CP), and a bare glassy carbon electrode (GCE) in the presence of 2 mM ruthenium hexamine/ 1 M potassium chloride mediator solution.

accessed by aqueous solutions, promoting their use in energy or sensing applications, including use with PSI-based systems.

As with the development of porous metal or semiconducting electrodes, the impact of porosity on electrochemical behavior can often obscure surface area-driven electrochemical measurements. Measuring changes in the capacitive behavior of the electrode can assist in characterizing changes to the electrochemically active surface area (ECSA) of a porous material.^[29] By plotting the increase in non-faradaic current at varying scan rates, the specific capacitance (F cm^{-2}) for the electrode can be obtained and used to measure changes in surface area between electrodes of similar composition (Figure 2). Flame treatment of the CP substrate resulted in a change to specific capacitance of nearly 170 times

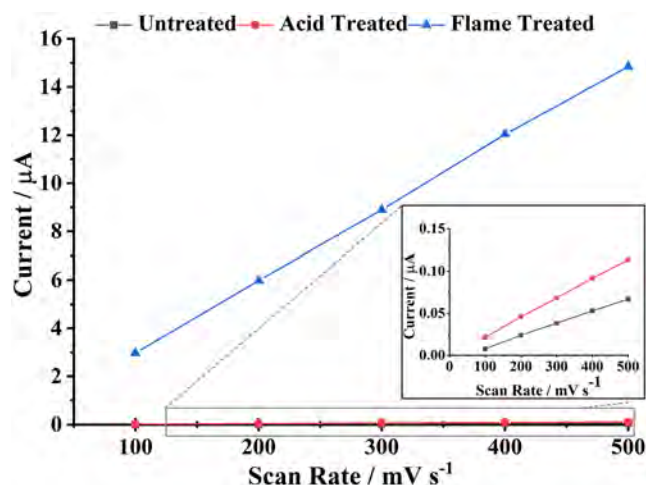


Figure 2. Linear graph of non-faradaic current observed in cyclic voltammetry plotted against the scan rate for untreated (inset), acid-treated (inset), and flame-treated CP electrodes.

that of untreated CP highlighting the immense increase in surface area following pretreatment of commercial CP materials.

These results support the surface area enhancement trends observed through faradaic current-based processes. As it stands untreated CP remains largely inaccessible to aqueous solutions detracting from its application in PSI-based biohybrid devices. Through simple and rapid pretreatment methods, CP electrodes can easily be converted into a usable, high surface area substrate in biohybrid solar energy conversion, serving as a metal-free alternative in energy-harvesting applications. The superior wettability, increased electroactive surface area, and minimal pretreatment requirements compared to AT-CP made FT-CP the modification method of choice for this work.

2.2. PSI Multilayers on CP Substrates

To demonstrate the viability of CP substrates in PSI-based photoelectrochemical devices, electrodes were coated with varying amounts of PSI using vacuum-assisted deposition, a common method for loading PSI or other biological species onto electrode surfaces.^[23,25,30] The resulting photocurrents of multilayered devices were anodic regardless of the mediator species (Figure 3A).

The mediators methyl viologen (MV), ruthenium hexamine (RuHex), and 2,3-dimethoxy-5-methyl-*p*-benzoquinone (ubiquinone-0; ubi) as well as oxygenated potassium chloride electrolyte preferentially accept photoexcited electrons from the stromal F_B^- reaction center which leads to excess buildup of reduced species at the working electrode. Anodic photocurrent is realized when the reduced mediator species is sequentially oxidized at the underlying electrode. Of the mediators tested ubi and RuHex showed the best improvement in photocurrent density at the surface of biohybrid films, which is attributed to greater overpotentials versus the F_B reaction center of PSI when compared to MV (Figure S3, Supporting Information). While RuHex exhibits the

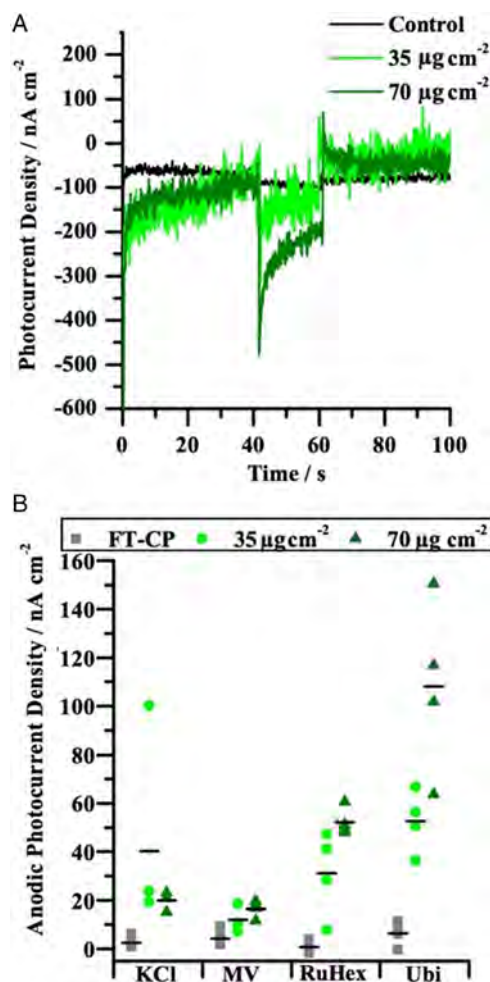


Figure 3. A) The resulting photocurrent behavior of Photosystem I (PSI) multilayers under different deposition amounts in the presence of a 2 mM ubiquinone mediator. B) Steady-state photocurrent densities of control and PSI multilayers on FT-CP in the presence of various mediators ($n = 4$). Average photocurrent densities are represented by a solid dash. The abbreviations for selected mediators are as follows: KCl—unmodified potassium chloride electrolyte; MV—methyl viologen dichloride; RuHex—ruthenium hexamine trichloride; Ubi—2,3-dimethoxy-5-methyl-*p*-benzoquinone.

greatest overpotential with respect to F_B^- , ubiquinone undergoes a two-electron transfer and has been well characterized as an electron acceptor from photosynthetic protein complexes pointing to its overall higher performance.^[31,32]

Inherent photoactivity was observed at FT-CP control devices; however, the magnitude of this current was negligible ($<5 \text{ nA cm}^{-2}$) compared to the photocurrent densities produced with PSI-modified electrodes. The shapes of the current profile exhibit time-dependent Cottrellian decay, indicating similar behavior of PSI on carbon fiber electrodes to multilayers assembled on conventional inorganic electrodes (Figure 3). Furthermore, the time-dependent decay indicates that diffusionally limited pathways are responsible for the sustained photocurrent, which directly benefit from increased electrode surface areas. Overall, PSI-modified CP electrodes produced significantly higher photocurrent

densities than unmodified CP substrates. When mediated with ubiquinone, the mean photocurrent density was $0.11 \text{ } \mu\text{A cm}^{-2}$, a 15-fold enhancement over bare FT-CP ($0.007 \text{ } \mu\text{A cm}^{-2}$). These results validate adequately treated CP substrates as suitable electrodes for isolated PSI, expanding what had previously been achieved using whole thylakoid systems.^[19,20]

2.3. Rapid Immobilization of PSI on CP Substrates through Electropolymerization

To fully utilize the high surface area of treated CP substrates in PSI immobilization, electropolymerization was used to entrap PSI within a conducting polymer scaffold formed in situ.^[21,33] As a result of their electrochemical growth, polymers used in electropolymerization are often inherently conductive, making them favorable for use in solar cells or other energy-related applications. Beyond PSI entrapment for solar energy conversion, this technique is also useful for the immobilization of enzymes and other sustainable components are useful for sensing, energy production, and fuel generation.

To successfully entrap PSI in a conductive, electrochemically polymerized layer on CP or treated CP substrates, all components must first be combined and exposed to sufficient electrical potential needed to drive polymerization. The conductive polymer PEDOT polystyrene sulfonate (PEDOT:PSS) was chosen for its optical transparency, low inherent photoactivity, and previously demonstrated success when used in PSI-based devices.^[25,34] To verify the occurrence of electropolymerization at the CP surface, substrates subjected to different treatment methods were exposed to both control and monomer-containing solutions and held at a constant potential of $+1.2 \text{ V}$ (vs Ag/AgCl) (Figure S4A, Supporting Information). The resulting charge transferred to the solution was compared to evaluate the extent of polymerization (Table 1).

CP electrodes produced higher net charges in runs containing EDOT and PSS when compared to exposure to a control solution of pure electrolyte (Table 1), indicating the occurrence of new faradaic processes tied to polymer formation. FT-CP consumed a 19-fold higher net charge over untreated CP indicating more extensive polymerization at hydrophilic surfaces. SEM images also confirm the more liberal growth of polymer off treated CP surfaces as compared to unmodified CP (Figure S5, Supporting Information). When polymerized in the presence of PSI, the total charge passed during polymerization remained largely unchanged, suggesting the presence of PSI protein did not significantly impede the growth of PEDOT:PSS (Figure S4B, Supporting Information).

Table 1. Mean charge delivered (mC) during a 40 s hold of fixed potential $+1.2 \text{ V}$ (vs Ag/AgCl) in the absence and presence of EDOT:PSS and PSI ($n = 3$).

	Control ^{a)}	PEDOT:PSS	PEDOT:PSS + PSI
CP	-0.18 ± 0.06	-0.68 ± 0.08	-0.49 ± 0.50
FT-CP	-3.4 ± 0.1	-13 ± 2	-9.8 ± 0.8

^{a)}Control electrodes prepared by following electropolymerization protocol in phosphate buffer only.

Protein films were formed using an electropolymerization solution composed of a 1:4 ratio of precursor solution (0.01 M EDOT and 0.1 M PSS) to extracted PSI solution, with control films substituting unmodified elution buffer for PSI extract. Higher ratios of PSI monomer than what have been used previously on planar electrodes were necessary to improve protein loading in the rapidly forming films due to higher surface area at treated carbon surfaces. Devices were tested in mediator solutions of 1 M KCl electrolyte. High-electrolyte concentrations were used to improve the overall performance of the devices, as lower concentrations of KCl lead to drifting dark photocurrents (I_{dark}) (Figure S6, Supporting Information). The drifting I_{dark} most likely stems from the high charging current associated with these high surface area, highly capacitive materials and should be accounted for when applying these materials to electrochemical systems.^[35]

Across the mediators tested, PSI-polymer films produced anodic photocurrent, consistent with results from vacuum-deposited protein. Photocurrent densities were calculated by taking the difference between average light photocurrent densities (J_{light}) and dark photocurrent densities (J_{dark}) before and after light exposure. Across most mediators, composites containing PSI outperformed PEDOT:PSS film devices fabricated on flame-treated CP (Figure 4).

The best performance was achieved in pure electrolyte solution, suggesting dissolved oxygen is effective at shuttling charge from the composite films to the underlying carbon electrode, with PSI-containing devices exhibiting a sevenfold increase in current density (-12 vs -87 nA cm⁻²). Relying on dissolved oxygen is not ideal for sustained photocurrent generation, however, as the formation of reactive oxygen species (ROS) can lead to protein and polymer degradation over extended performance.^[36] The next best electrolyte system was shown to be ubiquinone. Ubiquinone and other quinone derivatives are known to be natural electron acceptors in aerobic photosynthesis making them suitable candidates for PSI-based biohybrid devices.^[31]

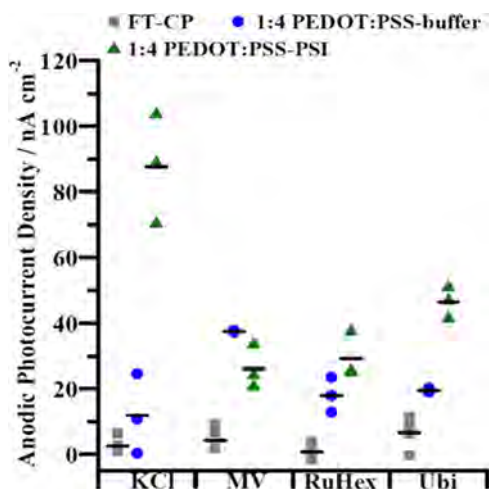


Figure 4. Photocurrent densities of composites formed on FT-CP substrates under potentiostatic conditions of +1.2 V for 40 s in 1 M KCl with no mediator, 2 mM MV, 2 mM RuHex, 2 mM ubiquinone ($n = 3$). Average photocurrent density values are represented by a solid dash.

To optimize the PEDOT:PSS-PSI composites prepared, alternative electropolymerization conditions were tested to maximize polymer growth and PSI intercalation. Using the same 1:4 ratio of monomer solution to PSI solution, increased polymerization times were tested at a constant +1.2 V (vs Ag/AgCl). As expected, the charge consumed and as such PEDOT:PSS grown increased proportionally with the polymerization time (Table 2); however, the photocurrent density barely increased (Figure 5).

Additionally, a potential sweep-based polymerization method (0 to +1.3 V vs Ag/AgCl potential window) was used in which the electrode was cycled between periods of electropolymerization (+0.9 to +1.3 V vs Ag/AgCl) and rest (+0.9 to 0.0 V vs Ag/AgCl). Under potential sweep electropolymerization, the quantity of polymer grown can be correlated to the number of growth-rest cycles performed, albeit with higher degrees of variance (Table 2).

The photoactivity of PEDOT:PSS controls prepared using a cycled potential method was higher than the photocurrent densities of films grown under potentiostatic conditions despite similar quantities of consumed charge during polymerization (Figure 5). Upon addition of PSI into the films, photocurrent densities of composites prepared using the cycled potential technique further increased well above the currents seen under potentiostatic growth. Increasing the number of cycles further improved the photoactivity and the deviation between devices.

Table 2. Mean charge delivered (mC) under different polymer growth conditions. PEDOT:PSS growth was achieved with either a set number of cycles between 0 and +1.3 V (vs Ag/AgCl) or for a set length of time at +1.2 V (vs Ag/AgCl) in the presence of PSI ($n = 3$).

	15 Cycles	30 Cycles	50 Cycles	40 s	80 s
Polymer	-39 ± 2	-69 ± 18	-98 ± 27	-16 ± 2	-35 ± 4
Polymer:PSI	-75 ± 30	-99 ± 25	-133 ± 21	-22 ± 1	-44 ± 1

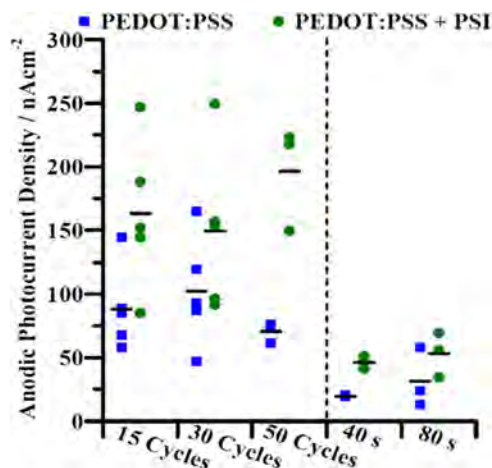


Figure 5. Photocurrent densities of poly(3,4-ethylenedioxythiophene) (PEDOT) and PEDOT-PSI composites on FT-CP. Composites were formed either using a potential sweep method (100 mV s⁻¹ scan rate from 0 V to +1.3 V for 15, 30, or 50 cycles) or potentiostatic conditions at varying times. All films were tested with a 2 mM ubiquinone/1 M KCl. Average photocurrent density values for the plotted device performances are represented by a solid dash.

Ultimately, devices subjected to 50 potential sweep cycles produced the highest photocurrent densities (-196 nA cm^{-2}), nearly a fourfold increase over PSI–PEDOT:PSS films prepared under an 80 s potential hold (-53 nA cm^{-2}) (Figure 5). The photocurrent density from these films also surpassed what was achieved with PSI multilayers prepared using vacuum-assisted deposition warranting the use of electropolymerization as a rapid, accessible method to prepare bioelectrodes.

PEDOT:PSS preparation using cyclic voltammetry seemed to have a more pronounced impact on the quality of protein–polymer composite. For one, the net charge consumed under potential sweep polymerization was greater than what was seen under potentiostatic growth, indicating higher densities of polymer at the electrode surface (Table 2). The photocurrent densities also surpassed what is expected solely based on the higher degree of polymerization, as evidenced between the electrodes prepared with 50 potential sweep cycles and those prepared under an 80 s potential hold. Whereas the charge consumed during electropolymerization increased by a factor of 3 for the two conditions, photocurrent densities increased nearly fourfold, suggesting further enhancement of the produced composites. Cycling the applied potential during electropolymerization likely aids in the mass transport of protein and monomer to the electrode surface, leading to higher photoactive polymer films and overall higher device performance as seen with other bioelectrodes prepared in a similar manner.^[37,38]

The photocurrent densities obtained at FT-CP substrates ($\approx 0.2 \text{ } \mu\text{A cm}^{-2}$) are comparable to PSI multilayers assembled on graphene ($0.5 \text{ } \mu\text{A cm}^{-2}$) and gold ($1.2 \text{ } \mu\text{A cm}^{-2}$) electrodes.^[15,39] While graphene oxide-coated substrates boast higher photocurrent densities overall ($4 \text{ } \mu\text{A cm}^{-2}$), protein films of a higher density than this study were used.^[16] Furthermore, the methods proposed in this study can be more readily applied in large-scale device assembly applications and are better suited for distributable energy production.^[15,16] Furthermore, the enhancement in photocurrent is greater than the increase in charge consumed during polymer growth pointing to a synergistic effect between the protein and polymer film. Additional factors such as increased protein loading likely contribute to photocurrent enhancement beyond increased polymer growth under dynamic polymerization conditions promoting their use in bioelectrode preparation. In conclusion, CP substrates open the door to disposable, affordable, metal-free bioelectrodes capable of scalable solar energy conversion.

3. Conclusion

CP was successfully utilized as an all-carbon, low-cost alternative to inorganic electrodes capable of sustaining photo-driven-mediated electron transfer at PSI multilayers. Prior to use, it is critical to pretreat CP substrates to maximize the accessible surface area through both the removal of any protective coating and the creation of hydrophilic moieties on the fibers surface. Simple treatments such as soaking in acid solutions or exposure to an open flame proved effective, with flame treatment improving the ECSA by a factor of roughly 10 for faradaic processes. PSI vacuum deposited on flame-treated CP produced a consistent anodic photocurrent ($0.11 \text{ } \mu\text{A cm}^{-2}$) using a ubiquinone mediator. More stable photoactive composites can be formed by entrapping PSI

within an electropolymerized composite, which capitalizes on the improved CP electrode surface area following pretreatment. Using cyclic voltammetry as a polymerization method, the produced photocurrent densities could be pushed to $0.22 \text{ } \mu\text{A cm}^{-2}$ under the conditions tested in this study. These methods can be readily employed to upscale the size of the produced photoactive electrode beyond benchtop dimensions with low-cost, all-carbon electrode materials.

4. Experimental Section

Chemicals and Materials: Toray CP-060 was purchased from the Fuel Cell Store (fuelcellstore.com) in $20 \times 20 \text{ cm}$ sheets. The CP sheets were covered with a standard 5% weight wet proofing layer of Teflon. Sheets were 0.19 mm thick, with a porosity of 78% and a resistivity of $80 \text{ m}\Omega \text{ cm}$ through the plane as reported by the manufacturer. Hydrochloric acid, sulfuric acid, sodium phosphate monobasic, potassium chloride (Fisher Scientific), 3,4-ethylenedioxythiophene (EDOT), poly(sodium 4-styrenesulfonate) (PSS), ruthenium hexamine (III) chloride (RuHex), ferricyanide, ferrocyanide, MV dichloride, 2,3-dimethoxy-5-methyl-*p*-benzoquinone (ubiquinone-0), triton X-100 (Sigma Aldrich) were procured and used as received. All deionized water (DI-water) was purified in-house (Millipore, 18 $\text{M}\Omega \text{ cm}$). Organic baby spinach from a local Kroger was used as the source of PSI for all experiments.

PSI Extraction: The method used to extract PSI has been previously described and is based on the protocols developed by Reeves and Hall.^[40] Fresh spinach was macerated in buffer to separate thylakoids from the rest of the leaves. After isolating the thylakoids from the remaining cell debris, Triton X-100 surfactant was added to release PSI from the membrane. The samples were once again centrifuged, and loaded through a hydroxyapatite column, trapping the PSI protein complex. The column was washed with a buffer solution to release the PSI protein under high-salt buffers. Samples were then stored in 2 mL aliquots at -80°C and dialyzed to remove surfactants and salts prior to use within experiments. PSI aliquots were measured to be $1 \text{ } \mu\text{M}$ in concentration following quantification with Baba's assay.^[41]

Electrode Preparation: Toray CP-060 was cut into rectangular electrodes, approximately $3 \times 2 \text{ cm}$. A tag of adhesive copper tape, 3 cm in length, was attached to one side of the electrode and used for electrical contact. The electrode was then covered with a PortHole inert electrochemical mask (Gamry Instruments) leaving a circular exposed area of 0.71 cm^2 . Electrodes pretreated with acid were briefly wetted with ethanol, then submerged in 0.1 M sulfuric acid for 5 min. Samples were rinsed with DI-water and allowed to dry. Additional CP electrodes were subjected to flame treatment instead, consisting of 5 s exposures to an open flame, followed by a DI-water rinse, and masking analogous to the previously discussed samples.

Electrochemical Measurements: All electronic measurements were conducted using a CH Instruments 660 A electrochemical workstation using a three-electrode setup with either modified CP or gold working electrode, a platinum mesh counter electrode, and an Ag/AgCl (1 M KCl) reference electrode. CVs of 2 mM RuHex in electrolyte solution consisting of 1 M KCl were obtained using CP electrodes subjected to different treatment methods as the working electrode.

Electropolymerization of polymer or polymer–PSI composites were prepared using a protocol modified from previous works.^[21] For PEDOT:PSS and PEDOT–PSI films, a monomer stock solution containing 0.01 M EDOT and 0.1 M PSS were combined with a 0.02 M phosphate buffer containing 0.001%wt Triton X-100 with or without PSI. The two solutions, denoted as solution A (EDOT & PSS) and solution B (eluted PSI or phosphate buffer) were combined 1:4 volumetrically unless otherwise specified. Films were polymerized either potentiostatically at $+1.2 \text{ V}$ (vs Ag/AgCl) for varied times or by cycling the working electrode potential between 0 and $+1.3 \text{ V}$ at a scan rate of 0.1 V s^{-1} for varied numbers of cycles.

Photochronoamperometry (PCA) was performed under applied potentials matching the open-circuit potential in either pure electrolyte or mediator solutions containing 2 mM RuHex, 2 mM MV, 5 mM sodium

ascorbate/250 μM 2,6-dichlorophenolindophenol, or 2 mM ubiquinone in 1 M KCl unless otherwise specified. During photocurrent measurements, electrodes were held in the dark for 40 s before illumination using a 100 mW cm^{-2} light source (KL 2500 LCD, Micro Optical Solutions, Newburyport, MA) with 20 s followed by another 40 s of darkness.

Electrochemical impedance spectroscopy (EIS) was performed in a solution containing 2 mM RuHex and 1 M KCl using a three-electrode configuration as described earlier. The potential was oscillated 10 mV above and below the measured open circuit potential (usually around -0.112 V vs Ag/AgCl) from 10 000 to 0.01 Hz. The relevant values were obtained from the resulting data by fitting with a Randles equivalent circuit.^[42,43]

Additional Instrumentation: Scanning electron microscopy of the samples was conducted using a Zeiss Merlin system with a GEMINI II column using a 2 keV accelerating voltage at working distance of 5 mm, with an InLens secondary electron detector.

All contact-angle measurements were made using a Rame–Hart goniometer. A static 1 μL drop of deionized water was added to each sample and the contact angle was measured at one side of the drop. Triplicate samples were measured for each reported condition and the average contact angle with standard deviation is reported.

Raman measurements were conducted on a Thermo Scientific DXR confocal Raman microscope. All measurements were made using a 532 nm laser under normal operation parameters.

Supporting Information

Supporting Information is available from the Wiley Online Library or from the author.

Acknowledgements

This work was supported by the U.S. Department of Agriculture (2019-67021-29857), National Science Foundation (DMR-1507505; DMR-0619789; CHE-1506587), and the Vanderbilt Institute of Nanoscale Science and Engineering (VINSE) NSF-REU (Grant no. 1560414). The authors would like to extend special thanks to VINSE for use of their instrumentation and lab space (NSF EPS 1004083).

Conflict of Interest

The authors declare no conflict of interest.

Data Availability Statement

The data that support the findings of this study are available from the corresponding author upon reasonable request.

Keywords

carbon, electrochemistry, photoelectrochemical cells, photoelectrochemistry, Photosystem I, Toray paper

Received: September 15, 2022

Revised: November 22, 2022

Published online: January 27, 2023

- [1] A. Agostiano, A. Ceglie, M. D. Monica, *Bioelectrochem. Bioenerg.* **1983**, 10, 377.
 [2] D. Gust, T. A. Moore, A. L. Moore, *Acc. Chem. Res.* **2009**, 42, 1890.
 [3] W.-J. Ong, L.-L. Tan, Y. H. Ng, S.-T. Yong, S.-P. Chai, *Chem. Rev.* **2016**, 116, 7159.

- [4] T. J. Meyer, *Acc. Chem. Res.* **1989**, 22, 163.
 [5] J. H. Golbeck, D. A. Bryant, *Curr. Top. Bioenerg.* **1991**, 16, 83.
 [6] J. H. Golbeck, *Annu. Rev. Plant Physiol. Plant Mol. Biol.* **1992**, 43, 293.
 [7] P. Fromme, P. Jordan, N. Krauß, *Biochim. Biophys. Acta* **2001**, 1507, 5.
 [8] A. Amunts, O. Drory, N. Nelson, *Nature* **2007**, 447, 58.
 [9] R. A. Grimme, C. E. Lubner, D. A. Bryant, J. H. Golbeck, *J. Am. Chem. Soc.* **2008**, 130, 6308.
 [10] C. E. Lubner, R. Grimme, D. A. Bryant, J. H. Golbeck, *Biochemistry* **2010**, 49, 404.
 [11] K. Hasan, R. D. Milton, M. Grattieri, T. Wang, M. Stephanz, S. D. Minter, *ACS Catal.* **2017**, 7, 2257.
 [12] K. H. Sjöholm, M. Rasmussen, S. D. Minter, *ECS Electrochem. Lett.* **2012**, 1, G7.
 [13] T. Wang, R. C. Reid, S. D. Minter, *Electroanalysis* **2016**, 28, 854.
 [14] D. S. Hecht, L.-B. Hu, G. Irvin, *Adv. Mater.* **2011**, 23, 1482.
 [15] D. Gunther, G. LeBlanc, D. Prasai, J. R. Zhang, D. E. Cliffl, K. I. Bolotin, G. K. Jennings, *Langmuir* **2013**, 29, 4177.
 [16] E. Darby, G. LeBlanc, E. A. Gizzie, K. M. Winter, G. K. Jennings, D. E. Cliffl, *Langmuir* **2014**, 30, 8990.
 [17] D. Ciornii, S. C. Feifel, M. Hejazi, A. Koelsch, H. Lokstein, A. Zouni, F. Lisdat, *Phys. Status Solidi A* **2017**, 214, 1700017.
 [18] S. Morlock, S. K. Subramanian, A. Zouni, F. Lisdat, *ACS Appl. Mater. Interfaces* **2021**, 13, 11237.
 [19] M. Rasmussen, A. Wingersky, S. D. Minter, *Electrochim. Acta* **2014**, 140, 304.
 [20] M. Rasmussen, S. D. Minter, *Electrochim. Acta* **2014**, 126, 68.
 [21] E. A. Gizzie, G. LeBlanc, G. K. Jennings, D. E. Cliffl, *ACS Appl. Mater. Interfaces* **2015**, 7, 9328.
 [22] E. A. Gizzie, J. S. Niezgoda, M. T. Robinson, A. G. Harris, G. K. Jennings, S. J. Rosenthal, D. E. Cliffl, *Energy Environ. Sci.* **2015**, 8, 3572.
 [23] D. Dervishogullari, E. A. Gizzie, G. K. Jennings, D. E. Cliffl, *Langmuir* **2018**, 34, 15658.
 [24] X. Xiao, M. E. Wang, H. Li, P. Si, *Talanta* **2013**, 116, 1054.
 [25] M. T. Robinson, C. E. Simons, D. E. Cliffl, G. K. Jennings, *Nanoscale* **2017**, 9, 6158.
 [26] Z. Zhang, H. Liu, J. Deng, *Anal. Chem.* **1996**, 68, 1632.
 [27] Y. He, X. Wang, H. Huang, P. Zhang, B. Chen, Z. Guo, *Appl. Surf. Sci.* **2019**, 469, 446.
 [28] D. J. Choi, A. Boscá, J. Pedrós, J. Martínez, V. Barranco, J. M. Rojo, J. J. Yoo, Y.-H. Kim, F. Calle, *Compos. Interfaces* **2016**, 23, 133.
 [29] D. Voiry, M. Chhowalla, Y. Gogotsi, N. A. Kotov, Y. Li, R. M. Penner, R. E. Schaak, P. S. Weiss, *ACS Nano* **2018**, 12, 9635.
 [30] K. D. Wolfe, D. Dervishogullari, C. D. Stachurski, J. M. Passantino, G. K. Jennings, D. E. Cliffl, *ChemElectroChem* **2020**, 7, 585.
 [31] V. M. Friebe, D. J. K. Swainsbury, P. K. Fyfe, W. van der Heijden, M. R. Jones, R. N. Frese, *Biochim. Biophys. Acta (BBA)* **2016**, 1857, 1925.
 [32] F. Zhao, K. Sliozberg, M. Rögner, N. Plumeré, W. Schuhmann, *J. Electrochem. Soc.* **2014**, 161, H3035.
 [33] E. A. Gizzie, J. Scott Niezgoda, M. T. Robinson, A. G. Harris, G. K. Jennings, S. J. Rosenthal, D. E. Cliffl, *Energy Environ. Sci.* **2015**, 8, 3572.
 [34] S. Kazemzadeh, G. Riazi, R. Ajeian, *ACS Sustainable Chem. Eng.* **2017**, 5, 9836.
 [35] N. G. Tsierkezos, U. Ritter, *Phys. Chem. Liq.* **2012**, 50, 661.
 [36] K. D. Wolfe, D. Dervishogullari, J. M. Passantino, C. D. Stachurski, G. K. Jennings, D. E. Cliffl, *Curr. Opin. Electrochem.* **2020**, 19, 27.
 [37] W. Schuhmann, C. Kranz, H. Wohlschläger, J. Strohmeier, *Biosens. Bioelectron.* **1997**, 12, 1157.
 [38] J.-C. Vidal, E. Garcia-Ruiz, J.-R. Castillo, *Microchim. Acta* **2003**, 143, 93.
 [39] P. N. Ciesielski, C. J. Faulkner, M. T. Irwin, J. M. Gregory, N. H. Tolks, D. E. Cliffl, G. K. Jennings, *Adv. Funct. Mater.* **2010**, 20, 4048.

- [40] S. G. Reeves, D. O. Hall, *Methods in Enzymology* (Ed: A. San Pietro) Vol. 69, Academic Press, Cambridge MA **1980**, pp. 85–94.
- [41] K. Baba, S. Itoh, G. Hastings, S. Hoshina, *Photosynth. Res.* **1996**, 47, 121.
- [42] A. J. Bard, L. R. Faulkner, *Electrochemical Methods - Fundamentals and Applications*, 2 ed., John Wiley & Sons, Inc, New York, NY **2001**.
- [43] G. K. Jennings, J. C. Munro, T.-H. Yong, P. E. Laibinis, *Langmuir* **1998**, 14, 6130.